The Astronomical Journal, 140:1462–1474, 2010 November doi:10.1088/0004-6256/140/5/1462

LENTICULAR GALAXIES AT THE OUTSKIRTS OF THE LEO II GROUP: NGC 3599 AND NGC 3626

O. K. Sil'chenko[1,2,4], A. V. Moiseev[3], and A. P. Shulga[1]
[1] Sternberg Astronomical Institute, Moscow 119992, Russia; olga@sai.msu.su, alina.shulga@gmail.com
[2] Isaac Newton Institute of Chile, Moscow Branch, Moscow, Russia
[3] Special Astrophysical Observatory, Nizhnij Arkhyz, Karachai-Circassia 369167, Russia; moisav@gmail.com
Received 2010 January 19; accepted 2010 August 14; published 2010 October 15

ABSTRACT

We have studied unbarred S0 galaxies, NGC 3599 and NGC 3626, the members of the X-ray bright group Leo II, by means of three-dimensional spectroscopy, long-slit spectroscopy, and imaging, with the aim of identifying the epoch and mechanisms of their transformation from spirals. Both galaxies have appeared to bear complex features obviously resulting from minor merging: decoupled gas kinematics, nuclear star-forming rings, and multi-tiered oval large-scale stellar disks. The weak emission line nucleus of NGC 3599 bears all signs of Seyfert activity, according to the line-ratio diagnostics of the gas excitation mechanism. We conclude that the transformation of these lenticular galaxies took place about 1–2 Gyr ago, through gravitational mechanisms unrelated to the hot intragroup medium of Leo II.

Key words: galaxies: evolution – galaxies: individual (NGC 3599, NGC 3626) – galaxies: structure

Online-only material: color figures

1. INTRODUCTION

Lenticular galaxies as a class were perhaps formed rather recently. Observations of clusters at intermediate redshifts, at $z = 0.2$–0.7, catch the moment when the dominance of spiral galaxies in clusters is replaced by the dominance of S0s (Dressler et al. 1997; Fasano et al. 2000) so it allows us to state that lenticular galaxies as a type have been formed near redshift $z \approx 0.3$–0.4, or 3–5 Gyr ago. The mechanism of the transformation of spirals into S0s is, however, still uncertain. The common point of view is that the environment is key to this transformation, but exactly what properties of the environment—hot medium, dense settlement, high pairwise velocities, or something else—play a role remains a topic of discussion. In past years, an idea has arisen that the environment where S0s formed indeed consisted of groups of galaxies, and later the groups brought S0s into the clusters when accreting onto them (Wilman et al. 2009; Just et al. 2010). If so, then the properties of lenticulars in groups represent a particular interest for identifying the mechanisms of their (trans-)formation.

Nearby groups are very inhomogeneous as far as their properties are concerned. They may be dominated by late-type or early-type galaxies, half of them contain hot X-ray gas and half of them lack it (Mahdavi et al. 2000), and the observed ranges of group masses and of galaxy velocity dispersions are also rather large—from 10^{12} to $10^{15}\,M_{\odot}$ and from 50 to 800 km s^{-1}, respectively (Ramella et al. 1997). Thus studying lenticular galaxies in nearby groups with a spread of properties may allow us to identify the most important drivers of their evolution—or to confirm a feeling that different paths exist for the transformation of a spiral galaxy into a lenticular one. We have already obtained some interesting results in this way. Lenticular galaxies in groups reveal serious inhomogeneity of their properties. In the groups NGC 5576 (Sil'chenko 1997; Sil'chenko et al. 2002) and Leo I (Sil'chenko et al. 2003), where X-ray intragroup gas is absent, the early-type galaxies demonstrate synchronous nuclear evolution and have rather young (2–3 Gyr old) nuclear stellar populations; perhaps this synchronity is a manifestation of the major role of recent gravitational interactions. In the group NGC 80 (Sil'chenko & Afanasiev 2008; Startseva et al. 2009), which looks quite relaxed and has a prominent X-ray gaseous halo, the centers of some lenticular galaxies are old (NGC 80, IC 1541, NGC 86) while the others (IC 1548, NGC 85) are young and seem to have (trans-)formed quite recently due to minor mergers. Though for several elder lenticulars we cannot exclude the major role of hydrodynamical mechanisms like ram pressure, the presence of "old" lenticulars at the outskirts of the group, and of the "younger" ones in the center inverse the whole picture of the galaxy assembly.

The group Leo II is in some sense a middle case: it possesses X-ray gas, but the whole structure of its X-ray halo is not very regular, with two prominent peaks at two central galaxies, the S0 NGC 3607, which is the brightest galaxy in the group, and its elliptical neighbor, NGC 3608 (Mulchaey et al. 2002). We studied the central galaxies of the group (Afanasiev & Sil'chenko 2007) and found the different central ages of stellar populations—very old in NGC 3607 and intermediate in NGC 3608—so in this group we saw no synchroncity of evolution. In this paper, we continue to analyze the structure and properties of the nuclear stellar populations of the group members—this time in two off-center lenticular galaxies of the group, NGC 3599 and NGC 3626. The global characteristics of the galaxies under consideration are listed in Table 1. NGC 3626 is famous for its counterrotating large-scale gaseous disk (Ciri et al. 1995; Garcia-Burillo et al. 1998; Haynes et al. 2000). The dwarf S0 NGC 3599 is not as famous; however, recently a mysterious X-ray flash in its center prompted a theory about a supermassive black hole having tidally disrupted a star (Esquej et al. 2008), though the galaxy has not been reported to have a noticeable active nucleus.

2. THE OBSERVATIONS AND DATA USED

Our study of the lenticular galaxies NGC 3599 and NGC 3626 presented here includes analysis of the structure of the galaxies and determination of the characteristics of the central stellar

[4] Guest Investigator of the UK Astronomy Data Centre

Table 1
Global Parameters of the Galaxies

Galaxy	NGC 3599	NGC 3626
Type (NED[a])	SA0:	(R)SA(rs)0+
R_{25}, kpc (NED)	7.1	7.8
B_T^0 (RC3[b])	12.70	11.62
M_B(RC3+NED)	−18.8	−19.9
$(B-V)_T^0$ (RC3)	0.86	0.81
$(U-B)_T^0$ (RC3)	0.32	0.30
V_r (NED) (kms^{-1})	832	1493
Distance (Mpc)	20.4[d]	20.0[d]
Scale (pc arcsec^{-1})	99	97
Inclination (LEDA[c])	28°	56°
P.A.$_{\rm phot}$ (LEDA)	...	156°
σ_* (kms^{-1}) (LEDA)	67	142

Notes.
[a] NASA/IPAC Extragalactic Database.
[b] Third Reference Catalogue of Bright Galaxies.
[c] Lyon-Meudon Extragalactic Database.
[d] Tonry et al. (2001).

populations. The former aim is achieved by photometric decomposition of the Sloan Digital Sky Survey (SDSS) images and by comparing the photometric and kinematical orientation angles. The latter piece of work is made by means of panoramic spectroscopy and by analysis of the color maps. The list of the raw observational data used is given in Table 2.

Photometric data that we analyze include *gri*-images from the Sixth Data Release of the SDSS (Adelman-McCarthy et al. 2008) for both galaxies, the *Hubble Space Telescope* (*HST*) two-color data for the central region of NGC 3599 (*HST*/WFPC2, F814W and F555W bands; Prop. no. 5999, PI: A. Phillips), together with our own *BV*-photometry for NGC 3626 undertaken with the focal reductor SCORPIO (Afanasiev & Moiseev 2005) of the Russian 6 m Big Telescope Alt-azimuthal (BTA) in the Special Astrophysical Observatory (SAO RAS).

Also, the focal reducer SCORPIO in the long-slit mode has been used to obtain a red-range spectrum of NGC 3599. We hoped to probe the radial extension of the ionized-gas emission in this galaxy, but the emission was found to be confined only to the very central part of the galaxy, $R < 10''$.

The panoramic spectroscopy was made with the integral-field spectrograph of the BTA Multi-Pupil Fiber Spectrograph (MPFS; Afanasiev et al. 2001); also we have involved the data from the William Herschel Telescope integral-field spectrograph SAURON (Bacon et al. 2001) retrieved from the open Isaac Newton Group Archive which is maintained as part of the CASU Astronomical Data Centre at the Institute of Astronomy, Cambridge.

Integral-field spectroscopy allows one to simultaneously obtain, in one exposure, wide-range spectra for hundreds of spatial elements (spaxels) covering a two-dimensional area on the sky. By observing galaxies with the integral-field spectrograph, we get a possibility of mapping various spectral characteristics of the light integrated on the line of sight (LOS): surface brightness, both for the stellar continuum and gas emission lines, LOS velocities and velocity dispersions (or, in a more general sense, line-of-sight velocity distribution, LOSVD, shape parameters), and equivalent widths of absorption lines which we express in the well-formulated Lick index system (Worthey et al. 1994). The MPFS operates on the fiber-lens principle, so it provides a large free spectral range, about 1500 Å with a spectral resolution of 3 Å by using the CCD EEV 42–40 of 2048 × 2048 format as a detector; the price is a small field of view, 16 × 16 spaxels, with the sampling of 1″ per spaxel. The SAURON operates in TIGER mode (Bacon et al. 1995) so it exposes a fixed narrow spectral range, 4800–5350 Å, but packs densely more than 1500 spectra covering 44 × 38 spaxels. The "blank sky" spectra are exposed simultaneously with the galaxy spectra, on the same detector; they are taken at 4′ from the field center by the MPFS and at 1.′7 from the field center by SAURON. After the necessary primary reduction steps—bias subtraction, flatfielding, individual spectra extraction, calibration onto the wavelength scale, and sky subtraction—we analyze every spectrum individually, and after deriving interesting spectral characteristics, we combine them into the maps of the galaxy regions studied. The star velocities and stellar velocity dispersions are calculated by cross-correlating galaxy spectra with the spectra of G8–K2-giant stars observed on the same nights, and with the spectra of the twilight sky which is of G2-type. Several templates are taken to estimate the sensitivity of the velocities derived for the possible template mismatch; it has appeared to be negligible under our approach. The gas velocities are measured by calculating the baricenter positions of emission lines. The Lick indices Hβ, Mgb, Fe5270, and Fe5335 are calculated from the individual galaxy spectra, corrected for the stellar velocity dispersion, and calibrated into the standard Lick system by using the observations of a dozen Lick standard stars (Worthey et al. 1994) observed by the same observational run as the galaxies—for a more detailed description of the procedure, see, e.g., Sil'chenko (2006) or Afanasiev & Sil'chenko (2007). The typical errors of the individual velocity measurements are of 10 km s^{-1}, the errors of the Lick indices vary between 0.1 Å in the centers of galaxies and 0.5 Å at the edges of the field of view.

3. THE LARGE-SCALE STRUCTURE OF NGC 3599 AND NGC 3626

We have analyzed the large-scale structure of the galaxies by applying the two-dimensional decomposition software BUDDA

Table 2
Spectroscopy and Photometry of the Galaxies Studied

Date	Galaxy	Exposure	Spectrograph	Field	P.A. (top)	Spectral Range	Seeing
2005 Apr 13	NGC 3599	100 minutes	BTA/MPFS	16″ × 16″	154.°5	4200–5600 Å	1.″5
2006 Apr 5	NGC 3599	60 minutes	BTA/MPFS	16″ × 16″	276°	5800–7200 Å	2.″0
2005 Apr 14	NGC 3626	60 minutes	BTA/MPFS	16″ × 16″	260.°5	4200–5600 Å	1.″5
2006 Apr 5	NGC 3626	30 minutes	BTA/MPFS	16″ × 16″	261°	5800–7200 Å	2.″0
2008 Jan 9	NGC 3626	60 minutes	WHT/SAURON	36″ × 41″	155°	4800–5350 Å	1.″7
2008 Feb 29	NGC 3599	60 minutes	WHT/SAURON	36″ × 41″	215°	4800–5350 Å	1.″1
2009 Apr 5	NGC 3599	30 minutes	BTA/SCORPIO/LS	1″ × 360″	240°	6100–7100 Å	1.″3
2005 Dec 25	NGC 3626	4 minutes	BTA/SCORPIO/IM	360″ × 360″	0°	*B* band	1.″8
2005 Dec 25	NGC 3626	6 minutes	BTA/SCORPIO/IM	360″ × 360″	0°	*V* band	1.″7

Table 3
Sérsic Parameters of the Brightness Profiles Fitting

Component	Radius Range of Fitting (arcsec)	n	P.A.$_0$	$1-b/a$	μ_0 (mag sq. arcsec^{-2})	r_0 (arcsec)	r_e (arcsec)
			NGC 3599, i-band				
Outermost disk	>60	1	52°	0.11 ± 0.05	20.6 ± 1.0	25 ± 4	...
Outer disk	30–60	1	53°	0.11 ± 0.05	20.8 ± 0.4	28 ± 4	...
Inner disk	10–35	1	101°	0.20 ± 0.01	19.5 ± 0.1	14.0 ± 0.6	...
Central bulge	<10	4.28 ± 0.45	94°	0.12 ± 0.01	...	...	3.18 ± 0.08
			NGC 3599, r-band				
Outermost disk	>60	1	52°	0.07 ± 0.04	20.6 ± 1.0	22 ± 3	...
Outer disk	30–60	1	55°	0.10 ± 0.05	21.4 ± 0.5	30 ± 4	...
Inner disk	10–35	1	101°	0.23 ± 0.03	19.9 ± 0.1	13.2 ± 0.7	...
Central bulge	<10	4.24 ± 0.50	95°	0.10 ± 0.01	...	...	3.14 ± 0.11
			NGC 3599, g-band				
Outermost disk	>60	1	52°	0.06 ± 0.03	21 ± 1.0	20 ± 4	...
Outer disk	30–60	1	57°	0.12 ± 0.00	22.0 ± 0.6	30 ± 5	...
Inner disk	10–35	1	102°	0.22 ± 0.03	20.4 ± 0.2	12.6 ± 0.7	...
Central bulge	<10	3.75 ± 0.53	81°	0.09 ± 0.01	...	...	2.77 ± 0.11
			NGC 3626, i-band				
Outer disk	>45	1	159°	0.31 ± 0.05	19.1 ± 0.5	21 ± 2	...
Inner disk	10–45	1	168°	0.48 ± 0.02	18.6 ± 0.1	19.8 ± 0.7	...
Central bulge	<10	2.1 ± 0.1	164°	0.32 ± 0.02	...	...	2.52 ± 0.05
			NGC 3626, r-band				
Outer disk	>45	1	160°	0.31 ± 0.05	19.5 ± 0.5	21 ± 2	...
Inner disk	10–45	1	168°	0.49 ± 0.02	19.0 ± 0.1	19.8 ± 0.6	...
Central bulge	<10	2.07 ± 0.10	164°	0.33 ± 0.02	...	...	2.47 ± 0.06
			NGC 3626, g-band				
Outer disk	>45	1	164°	0.32 ± 0.06	20.4 ± 0.6	24 ± 2	...
Inner disk	10–45	1	169°	0.50 ± 0.02	19.8 ± 0.1	21.6 ± 0.7	...
Central bulge	<10	1.73 ± 0.21	163°	0.35 ± 0.02	...	...	2.73 ± 0.06

(de Souza et al. 2004) to the images taken from the SDSS DR6 and then sky subtracted. The results of decomposition in three bands, g, r, and i, are given in Table 3. The present version of BUDDA allows us to decompose a galaxy into an exponential disk and a bulge described by the Sérsic profile with an arbitrary power parameter. However, we know that an exponential scale length may vary along the radius—disks may be two-tiered, truncated, or antitruncated (Pohlen & Trujillo 2006; Erwin et al. 2008). To catch this peculiarity of the structures, we apply a more complex approach to the galaxy decompositions. Based on isophotal analysis, we define an outer zone where the outer disk dominates (i.e., the zone where the isophote position angle (P.A.) and ellipticity are constant along the radius), mask the inner part of the galaxy, and for the first time apply the BUDDA procedure only to the outer-disk-dominated zone. After obtaining the parameters of the outer disk, we subtract the full-extension model disk image from the original image of the galaxy and then apply BUDDA to the residual images to derive the parameters of the inner disk and of the bulge. For NGC 3599, we have been forced to repeat this procedure: this galaxy has appeared to possess a three-tiered disk, with the middle scale length being the longest. The isophote analysis has been made in the framework of IRAF.[5]

Figures 1 and 2 present the results of the isophote analysis in one of the filters for NGC 3599 and NGC 3626, respectively (the isophote behaviors in all filters are similar): the left plots refer to the galaxies as a whole and the right plots refer to the galaxies with the outer disks subtracted. Figures 1 (left) and 2 (left) demonstrate a common feature: there exists a transition radius where the major axis P.A.s change abruptly and the ellipticities drop. At the same radii, the disk profiles have breaks in the slopes. The isophote-analysis results for the surface brightness distribution in NGC 3599 consistent with those presented in Figure 1 have been obtained by Magrelli et al. (1992) in the V band. Here we place the isophote-analysis results for NGC 3599 and NGC 3626 together to point out the similarity of their structures.

We suggest that in Figures 1 and 2 we see transitions between the inner and outer disks (as for the third disk in NGC 3599 we can treat it as a truncated portion of the outer disk because it has the same P.A. and ellipticity and differs only by scale length). We propose the following arguments for treating the inner exponential structures with the high isophote ellipticities as quite separate inner disks and not as bars within the single-exponential (outer) disks. First, within the inner-disk zones the isophotes demonstrate nearly constant high ellipticities, with low-contrast maxima at the inner edges corresponding to the possible stellar rings (Figures 1 (left) and 2 (left)), while bars, having flat brightness profiles in early-type galaxies (Elmegreen & Elmegreen 1985), being superposed onto the exponential-profile disks would force the ellipticities to rise constantly along the radius toward the bars' ends (Wozniak et al. 1995). Second, over the extension of the inner disks the surface brightness profiles demonstrate a regular exponential shape with scale lengths significantly smaller than those of the outer disks

[5] IRAF is distributed by the National Optical Astronomy Observatory, which is operated by the Association of Universities for Research in Astronomy, Inc., under cooperative agreement with the National Science Foundation.

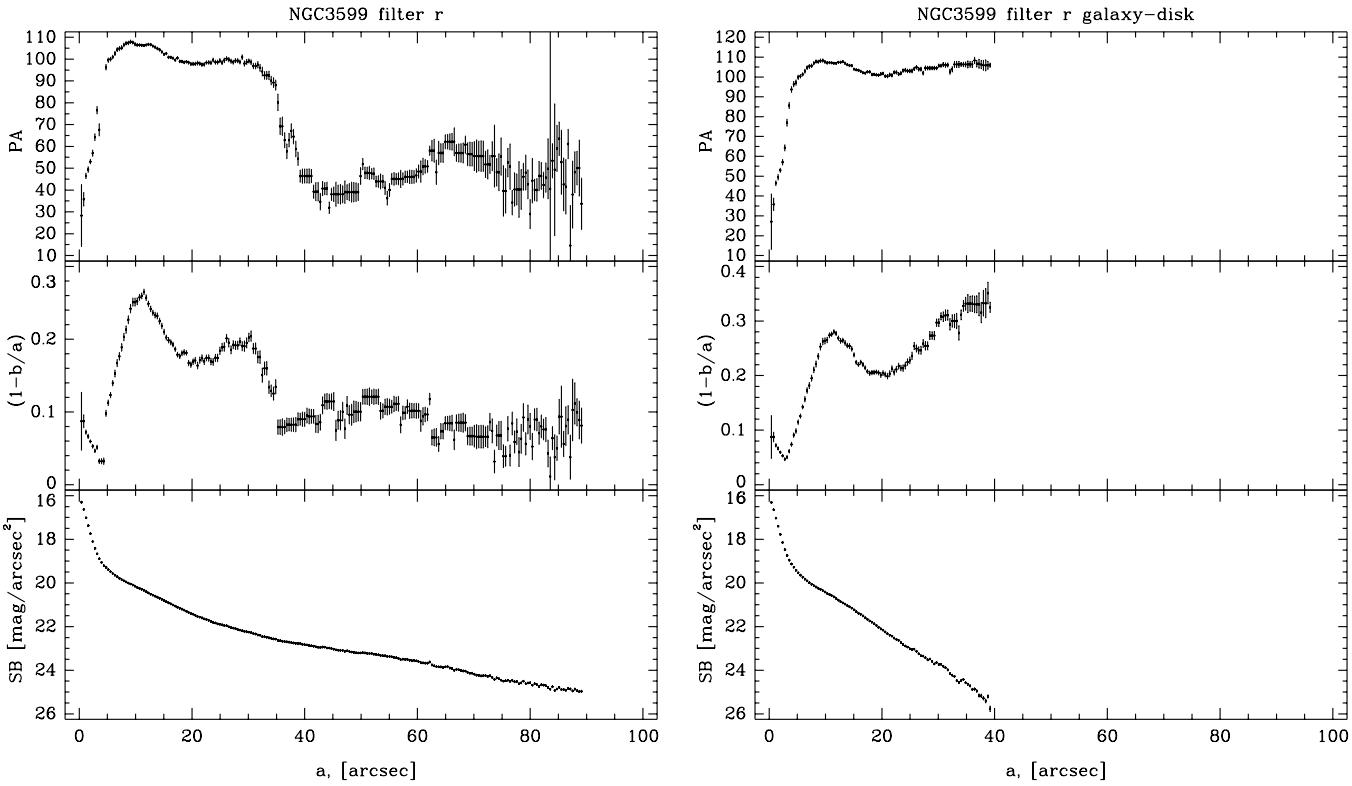

Figure 1. Results of the isophotal analysis for the *r*-band image of NGC 3599 for the full image (left) and for the residual image after subtracting the model outer disk (right). In both plots, the position angle of the isophote major axis is shown in the top panels, the ellipticity is shown in the middle panels, and the azimuthally averaged surface brightness profiles are given in the bottom panels.

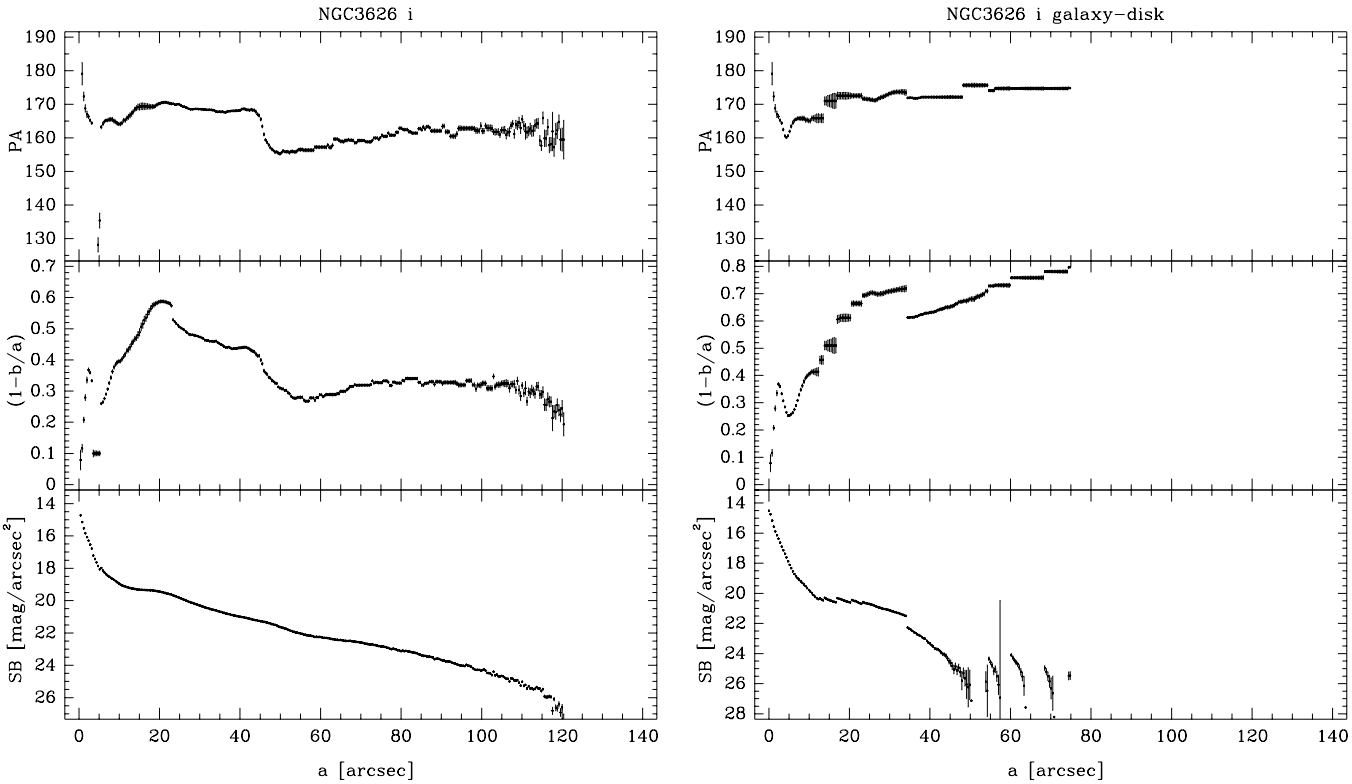

Figure 2. Results of the isophotal analysis for the *i*-band image of NGC 3626 for the full image (left) and for the residual image after subtracting the model outer disk (right). In both plots, the position angle of the isophote major axis is shown in the top panels, the ellipticity is shown in the middle panels, and the azimuthally averaged surface brightness profiles are given in the bottom panels.

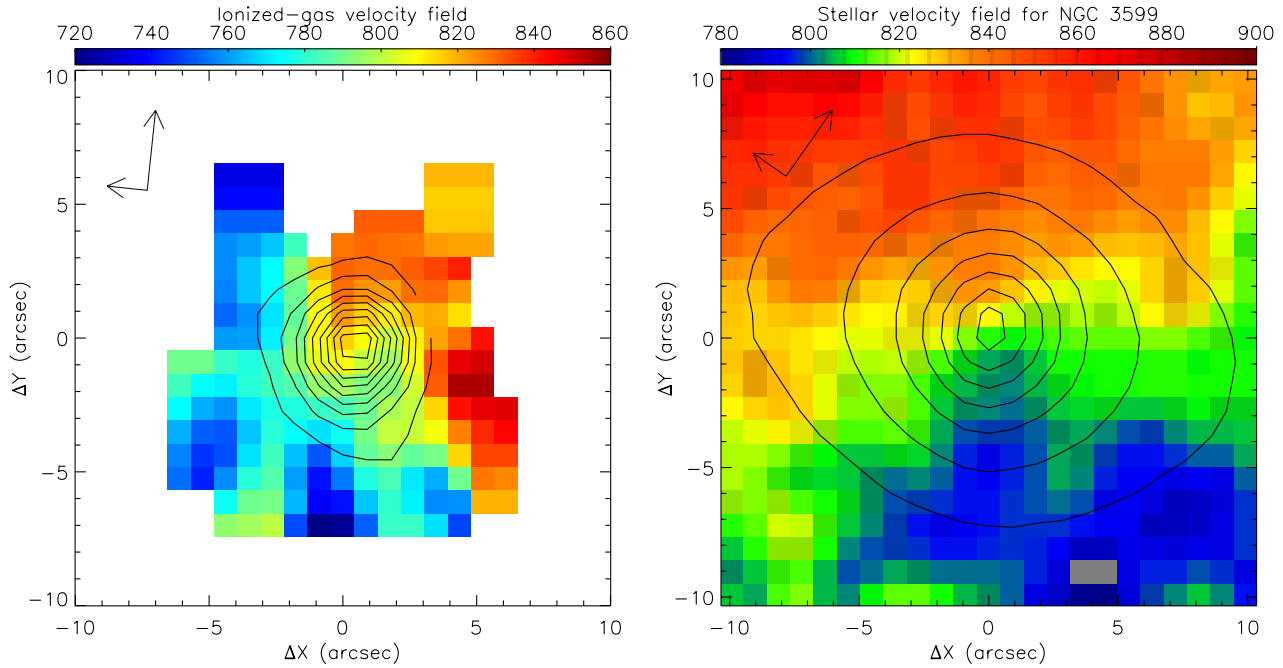

Figure 3. Line-of-sight (LOS) velocity fields for NGC 3599. Left: the LOS velocity field of the ionized gas from MPFS; right: the LOS velocity field of the stars from SAURON. The long arrow is directed toward the north, and the short is directed one toward the east.

(A color version of this figure is available in the online journal.)

(the steeper slopes). In the barred single-exponential disks, the azimuthally averaged surface brightness profiles are very smooth, with little, if any, influence of the ends of bars on the profile slopes (Elmegreen & Elmegreen 1985; Elmegreen et al. 1996). Thus we conclude that the photometric analysis implies the presence of inner, separate stellar disks in both NGC 3599 and NGC 3626; in NGC 3599 it is a pure exponential-profile structure (Figure 1 (right)), while in NGC 3626 a sort of a flat-profile lens may also be present (Figure 2 (right))—see also the decomposition of NGC 3626 by Laurikainen et al. (2005). If we assume that the outer isophote P.A.s and ellipticities relate to the orientation of the line of nodes and to the cosine of inclination of the galaxy symmetry planes, respectively—and it is so, if the outer disks are round—then the inner disks must be oval, or round but inclined to the planes of the outer disks. To choose between these alternatives, we need kinematical data: the photometry alone cannot discriminate between these two configurations.

4. THE KINEMATICS OF THE CENTRAL PARTS OF NGC 3599 AND NGC 3626

To compare the kinematics of the stars and of the ionized gas, we involve both the data from MPFS and from SAURON. The SAURON field of view is larger than that of the MPFS, but SAURON observes only the green spectral range where the strongest emission line, [O III]λ5007, is still hardly measurable while sinking to the bottom of the prominent Ti I absorption line. MPFS provides us with the measurements of the emission line [N II]λ6584 which is strong and free of underlying absorptions and so gives us the most reliable velocity fields for the warm gas component. The SAURON *stellar* velocity fields are preferred due to their larger field of view. We apply a tilted-ring analysis to both gaseous and stellar LOS velocity fields by using the software DETKA (Moiseev et al. 2004), which estimates both the P.A. of the kinematical major axis and the inclination of the rotation plane.

Figure 3 shows the LOS velocity fields for the stars and for the ionized gas in NGC 3599. The first visual inspection gives evidence for the orthogonality of the stellar and gaseous rotation. Indeed, while the kinematical major axis of the stellar component in the center of the galaxy is aligned at P.A.$_0$(stars) $\approx$ 50°, the emission-line measurements both from the [N II] and the [O III] data indicate P.A.$_0$(gas) $\approx -30°$ to $-50°$ at $R = 2''$–$5''$. By applying DETKA to the SAURON stellar velocity field, we have obtained radial variations of the orientation angles up to $R = 17''$ (Figure 4). There are no sure signs of the tilt of the stellar rotation plane. It is seen close to face-on, with the inclination estimates being $28° \pm 6°$ and the P.A.$_0$(kin) estimates —between 45° and 65° (rather poorly restricted because of the close to face-on rotation plane orientation). For the gas, we see a certain rotation-plane tilt: it is close to the stellar rotation plane near the center and is inclined by $\Delta i = 50° \pm 10°$ to it at $R > 6''$. The latter configuration may be a nearly polar gas ring which warps to the galactic plane near the very center. In Figure 4, we compare the orientations of the photometric and kinematical major axes: it is the way to check an axisymmetry of the galaxy potential, since within the axisymmetric potential the rotation must be circular, and the kinematical and photometric major axes of round disks must coincide. For NGC 3599, we see that the central part, $R < 3''$, demonstrates axisymmetric stellar rotation around the axis orthogonal to the plane in which the line of nodes coincides with the line of nodes of the outer disk (Table 3). In the inner disk area, within $R = 5''$–$15''$, the stellar kinematical major axis oscillates weakly near the line-of-node orientation while the isophotes turn by some 50°. Given this behavior of the photometric and kinematical major axes we can state that the inner disk in NGC 3599 is certainly oval.

Figure 5 presents the kinematical MPFS and SAURON maps for NGC 3626. The large-scale gaseous disk in this galaxy is known to counterrotate the stars (Ciri et al. 1995; Haynes et al. 2000). We analyze here the rotation and other motions of the central gas within $R < 17''$. In Figure 5, bottom, right we

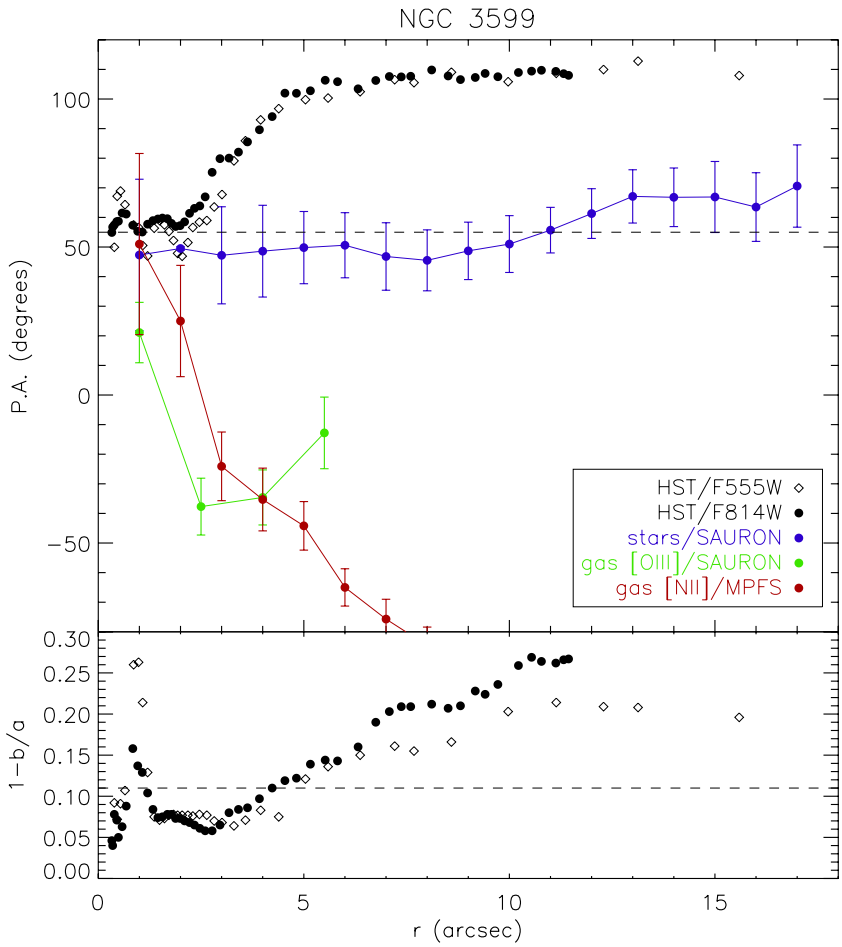

Figure 4. Comparison of the photometric and kinematical major axes in the central part of NGC 3599 (top), together with the high-resolution isophote ellipticity profile (bottom).

(A color version of this figure is available in the online journal.)

have masked the regions of the ionized-gas velocity field where the intensity of the emission line [O III]λ5007 is low, and so velocity measurements are uncertain. After that masking, the whole rotation of the highly excited warm gas can be separated into two distinct components: a counterrotating subsystem at $R > 8''$ which is already known and an orthogonally projected gaseous ring at $R < 7''$ which has not been reported yet. We note an interesting detail: the approaching "spot" of the ring is accompanied by the rise of the stellar velocity dispersion (Figure 5, top right). The most natural explanation of this local effect is a superposition of two stellar subsystems with slightly different LOS velocities. In other words, the inner gaseous ring has a stellar counterpart. Previous studies of the gas kinematics in the center of NGC 3626 have already given some hints regarding the multiple gas subsystems within $R \approx 10''$. Haynes et al. (2000) made two long-slit cross-sections—along major (P.A. = 157°) and minor (P.A. = 67°) isophote axes of NGC 3626. They noted double-peaked profiles of the [N II]λ6583 emission line inside the radius of $R \approx 6''$ which they treated as the simultaneous presence of the corotating and counterrotating gas at these radii. However, the warm gas is a collisional dynamical subsystem, so two *coplanar* gaseous disks with opposite rotation senses cannot exist. Also, the [N II]λ6583 LOS velocity profile obtained by Haynes et al. (2000) along the minor axis revealed deviations from the zero level of $\pm 100\,\mathrm{km\,s^{-1}}$ just inside $R \approx 6''$ (see their Figure 7, bottom plot). It means that the secondary gas component detected by Haynes et al. (2000) does not rotate circularly together with the stars in their symmetry plane. Furthermore, a careful inspection of the interferometric data for the molecular gas CO(1–0) presented by Garcia-Burillo et al. (1998), which have a spatial resolution of $3\farcs6 \times 2\farcs9$, has revealed that Garcia-Burillo et al. (1998) also noticed the traces of this circumnuclear gas subsystem. They report the presence of "anomalous components" that "could be attributed to corotating gas" (p. 240), which accounts for about 2.5% of all molecular-gas emission. They called this component "corotating" because they saw its contribution to the position–velocity (PV) diagram taken along the major axis: in the radius range of $R = 0''$–$4''$ it demonstrated the motions corotating with the stellar ones, with the amplitudes of $\Delta v = 180\,\mathrm{km\,s^{-1}}$—see their Figure 6, top. Over an even larger extension, up to $R = 8''$–$10''$, this anomalous component is seen in the PV diagram along the *minor* axis, and with the same amplitude of $\Delta v = 180\,\mathrm{km\,s^{-1}}$ (their Figure 6, bottom) as the "orthogonally rotating" component of [O III]λ5007 in our Figure 5, bottom right. Garcia-Burillo et al. (1998) explained their finding of the "anomalous gas motions" by possible strong non-circular motions—namely, by inflow through the circumnuclear spiral density wave. But we think that a gas inflow with a velocity of more than $200\,\mathrm{km\,s^{-1}}$ in the galaxy lacking a noticeable active nucleus seems to be incredible. Our interpretation, outlined below, would perhaps be more appropriate.

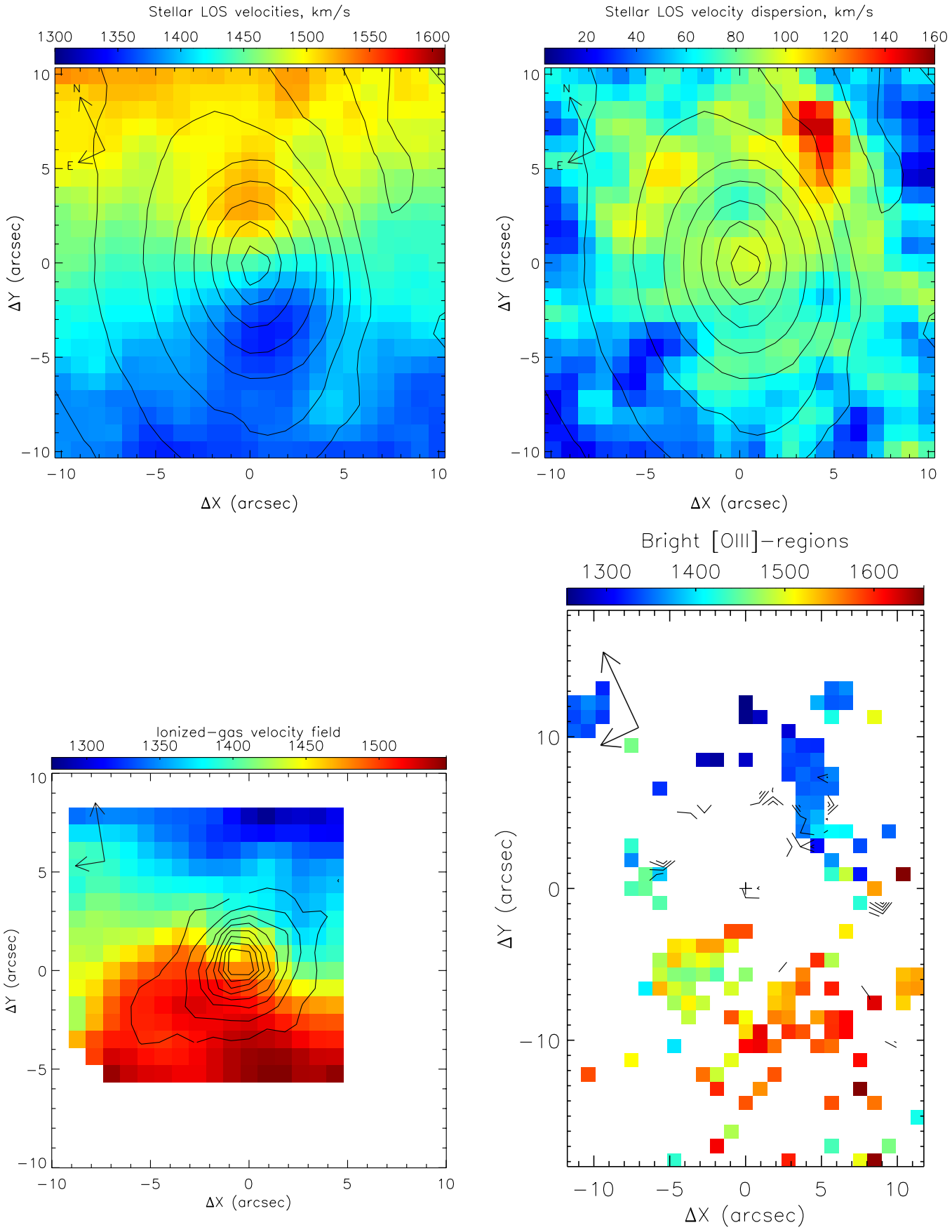

Figure 5. Line-of-sight (LOS) velocity fields for NGC 3626. Top left: the LOS velocity field of the stars from SAURON; top right: the stellar LOS velocity dispersion from SAURON; bottom left: the LOS velocity field of the ionized gas by the [N II] emission line from MPFS; bottom right: the same, by the [O III] emission line from SAURON. The long arrow is directed toward the north, and the short one is directed toward the east.

(A color version of this figure is available in the online journal.)

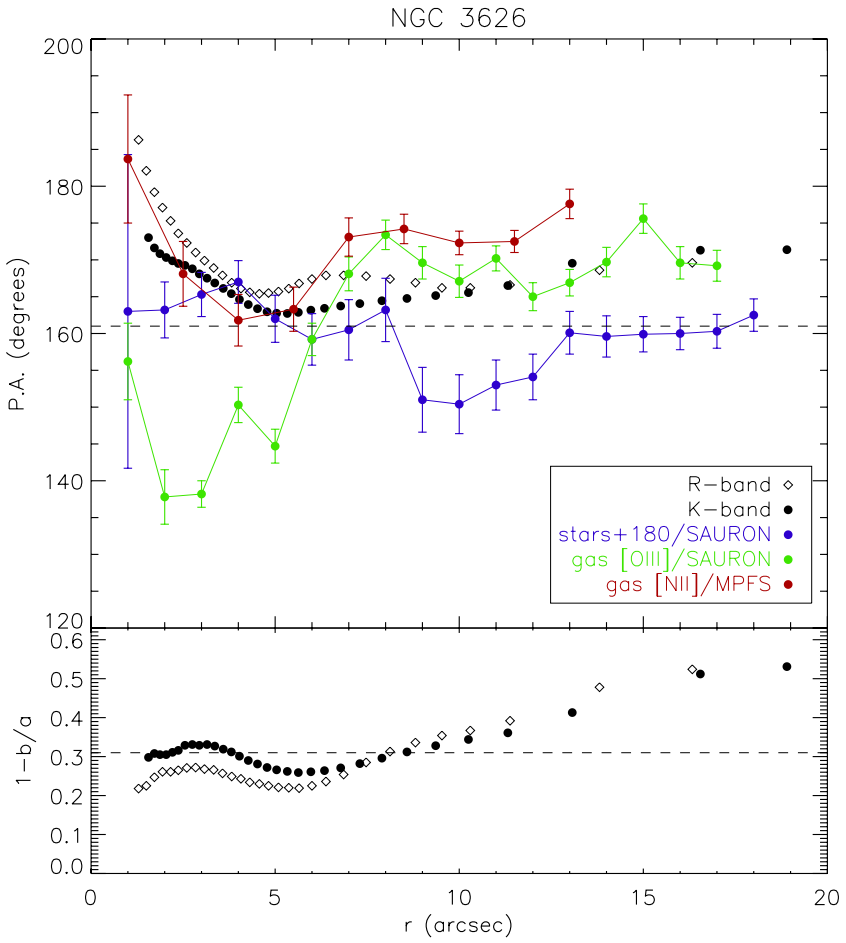

Figure 6. Comparison of the photometric and kinematical major axes in the central part of NGC 3626 (top), together with the isophote ellipticity profile (bottom). (A color version of this figure is available in the online journal.)

In Figure 6, we combine the data on photometric and kinematical major axes, both for the stars and for the ionized gas of NGC 3626. The stellar velocity field reveals the presence of a separate circumnuclear stellar component; the tilted-ring analysis shows that its kinematical orientation is close to the orientation of the outer large-scale stellar disk: $\mathrm{P.A.}_0(\mathrm{kin}) = 341^\circ \pm 5^\circ$ and $i = 32^\circ \pm 6^\circ$. The slight discrepancy in the kinematical inclinations of the outer disk and the circumnuclear stellar region, keeping in mind their similar isophote ellipticities, may imply that the latter is in fact a rather hot bulge. At $R \approx 8''$–$12''$ the stellar kinematical major axis deviates from the outer line of nodes; this deviation is due only to a couple of peculiar spots on the stellar velocity field which are related to the high-velocity dispersion regions and also perhaps to "accreted" stars superposed onto the main stellar component. Otherwise, the kinematical major axis of stars is quite stable at the outer line of nodes, which is very strange because the isophote major axis within the same radius range disagrees with the outer-disk line of nodes. The situation looks the same as in NGC 3599, but the gas behavior in NGC 3626 is even stranger. The gas kinematical major axis turns together with the continuum isophote major axis following its waving pattern; in the very center they both reach P.A. $\approx 190^\circ$. If we use the $\mathrm{P.A.}_0$ and i values provided by DETKA for the gas rotation plane orientation and compare them to the orientation parameters of the stellar disk, we obtain two solutions for the angle Δi between two planes: it is 58° or 87°. In other words, at radius $R < 4''$–$5''$ (400–500 pc), we observe perhaps an inner gas polar ring. At larger radii, $R > 7''$, the bulk gas kinematical major axis stabilizes around P.A. $= 170^\circ$–175° which agrees perfectly with the orientation and rotation of the outer neutral-hydrogen ring beyond the optical body of the galaxy (Haynes et al. 2000); this is not surprising because the outer neutral and the intermediate-radius warm gas have the same rotation sense, counterrotating with respect to the stars, and both gaseous subsystems are obviously related by their origin.

5. STELLAR POPULATIONS AND STAR FORMATION IN THE CENTERS OF NGC 3599 AND NGC 3626

The Lick index system is well calibrated on the MPFS data (Sil'chenko 2006) due to the wide spectral range and regular observations of the standard Lick stars under the standard spectrograph configuration. The SAURON spectral range is narrower than that of the MPFS so some problems with the absorption-line index calibrations exist (Kuntschner et al. 2006). We accept that the SAURON data are good for estimating qualitative index distributions over the galaxy area under consideration, while the MPFS data are good for making quantitative estimates of the stellar population properties in the very centers of the galaxies.

Figure 7 presents the index–index diagrams for NGC 3599 and NGC 3626 where we compare our MPFS data with the single stellar population (SSP) models by Thomas et al. (2003). The top panels of Figures 7 demonstrate the fair solar magnesium-to-iron ratio in both galaxies, and this ratio does

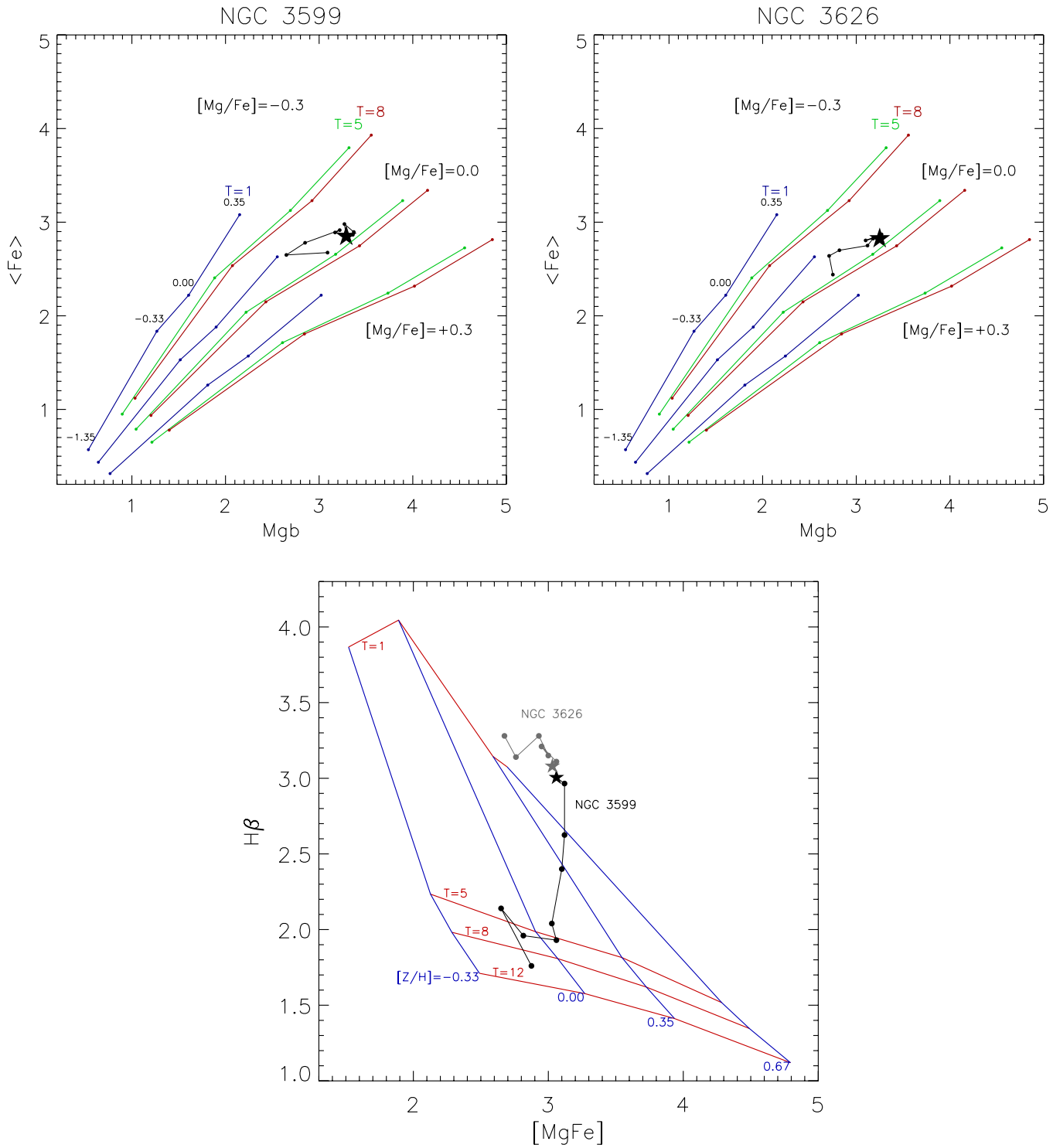

Figure 7. Top: ⟨Fe⟩ vs. Mgb diagrams for NGC 3599 and NGC 3626 azimuthally averaged index measurements. The black points are taken with the radial step of 1 arcsec, starting from the nuclei plotted by the large stars. The accuracy of the ring-averaged indices is 0.1 Å–0.15 Å. The simple stellar population models by Thomas et al. (2003) for three different magnesium-to-iron ratios (−0.3, 0.0, and +0.3) and three different ages (1, 5, and 8 Gyr) are plotted for reference. The small signs along the model curves mark the metallicities of +0.35, 0.00, −0.33, and −1.35, if one takes the signs from right to left. Bottom: age-diagnostic diagram for the stellar populations in the central parts of the galaxies under consideration; the Hβ-index measurements are rectified from the emission contamination as described in the text. The typical accuracy of the indices is 0.1 Å for the combined metal-line index and 0.15 Å for the Hβ. The stellar population models by Thomas et al. (2003) for [Mg/Fe] = 0.0 and four different ages (1, 5, 8, and 12 Gyr, from top to bottom curves) are plotted as reference frame; the dashed lines crossing the model curves mark the metallicities of +0.67, +0.35, 0.00, −0.33 from right to left.

(A color version of this figure is available in the online journal.)

not vary along the radius within 8″ from the centers. In the framework of the modern chemical evolution models, it means that the duration of the main, or of the last, star formation epoch in the central regions of the galaxies was longer than at least 1 Gyr everywhere including in the nuclei. In the bottom panel of Figure 7, comparing the Hβ-index to the combined metal-

line index allows us to simultaneously estimate the luminosity-weighted metallicity and the age of the stellar populations. Here two galaxies look somewhat different even though the ages of their nuclei coincide (they are 1–1.5 Gyr old or slightly younger). The environment of the young stellar nucleus in NGC 3599 is evidently older: at $R > 3''$ the SSP age rises to 5 Gyr at least, and the metallicity drops from several times solar to a subsolar one. In NGC 3626, the SSP age stays at a level of 1 Gyr up to the radial distance of $\sim 7''$ where the emission-line intensities increase dramatically, and the age estimates become somewhat uncertain.

In Figure 7, bottom, we have plotted the Hβ indices corrected for the modest emission contamination. We have calculated the corrections by using our red-range spectroscopic data of the MPFS. Our approach is based on the fact that the Hα emission line is always much stronger than the Hβ emission line while the equivalent widths of Balmer absorption lines are comparable, and for the intermediate-age stellar populations the Hα absorption is even weaker than for the higher-order lines (Balinskaya & Sil'chenko 1993). Moreover, the Balmer emission-line intensity ratios are narrowly fixed by the mechanism of gas excitation; for example, the lowest ratio $I(\mathrm{H}\alpha)/I(\mathrm{H}\beta)$, 2.5, is for the gas excitation by young massive stars (Burgess 1958), while shock excitation and excitation by power-law continuum (by active galactic nuclei (AGNs)) give a higher $I(\mathrm{H}\alpha)/I(\mathrm{H}\beta)$ ratio. Thus we have measured the equivalent widths of the Hα emission lines in the MPFS red spectra coadded over rings centered onto the galactic nuclei and have obtained EW(Hα *emis*) as a function of the distance from the centers. Then, to obtain the Hβ index corrections for the nuclei of NGC 3599 and NGC 3626, we have divided the measured EW(Hα *emis*) by 4 following the empirical prescription by Stasinska & Sodré (2001) for the combined mechanisms of gas excitation. For the region of NGC 3626 at $R \geqslant 4''$ we have used the coefficient of 2.7 because it is a site of the ongoing star formation as we shall see below. Over the off-nuclear region of NGC 3599 the emission lines are weak, and the corrections are applied only within $R \leqslant 2''$.

Because of the need to correct the Hβ index, we have analyzed the gas excitation mechanisms for the central regions of NGC 3599 and NGC 3626 in the manner of Veilleux & Osterbrock (1987), by calculating the emission-line intensity ratios. By measuring the SCORPIO spectra for NGC 3599, we have applied the Gauss analysis to the combination of the Hα absorption and emission lines; to measure [O III]λ5007 at the bottom of the Ti Iλ5007 absorption line we have used the SAURON spectra coadded in rings. The results are astonishing. The nucleus of the dwarf lenticular galaxy NGC 3599 demonstrates $I([\mathrm{O\,III}])/I(\mathrm{H}\beta) > 3$, $I([\mathrm{N\,II}]\lambda6584)/I(\mathrm{H}\alpha) = 2.15$, and $I([\mathrm{S\,II}]\lambda6717+6730)/I(\mathrm{H}\alpha) = 0.48$; in other words, according to the modern criteria by Kewley et al. (2006, see their Figure 4, middle), the nucleus of NGC 3599 is classified as a Seyfert nucleus. This is the second piece of evidence for the presence of a supermassive black hole in the center of this dwarf galaxy, after the discovery of the X-ray burst by Esquej et al. (2008). Within the radius of $2''$ from the center of NGC 3599 where the emission lines are still well measurable, their ratios remain far from the criteria for excitation by young stars and instead provide evidence of AGN excitation or shock excitation. We do not see any signs of star formation in the emission-line spectra of NGC 3599, but the color map of the galaxy provided by *HST* imaging (Figure 8) reveals a spectacular blue ring, with a radius of $1''.7$ and a color difference of about $\Delta(V-I) \approx 0.25$ with respect to the galaxy center. Since we do not see H II-type

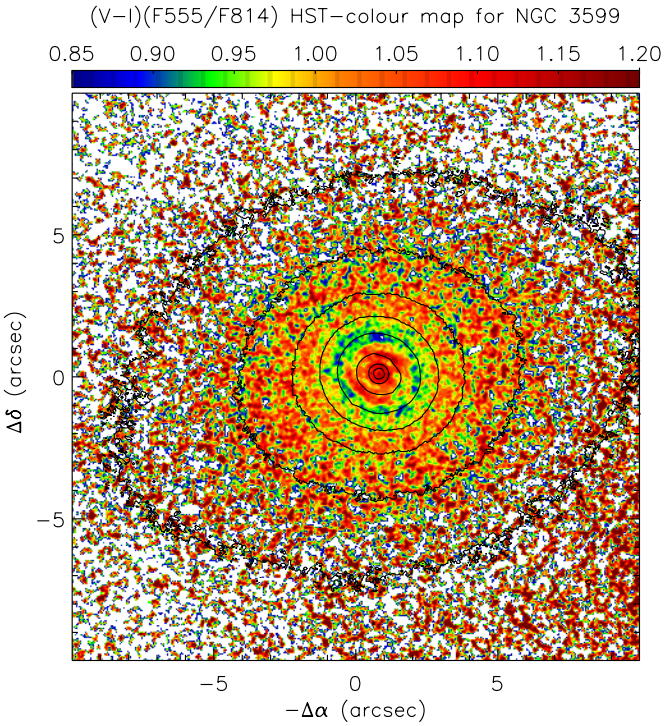

Figure 8. *HST* color map for the central part of NGC 3599; the isophotes superposed are from the F814W image.

(A color version of this figure is available in the online journal.)

excitation, the age of the starburst in the ring must be more than 10 Myr.

NGC 3626 has also rings of young stars in the central part. The $B-V$ color map (Figure 9, left) demonstrates an inhomogeneous oval blue zone, with the bluest points, $B-V \approx 0.7$–0.75, in $3''$ to the northeast and in $5''$ to the northwest. The mean stellar age within this zone, according to Figure 7, is about 1 Gyr. However, just beyond the outer radius of this blue ring the intense Hα emission arises, and at $R = 7''$ to the north we see an emission-line ratio $I([\mathrm{N\,II}]\lambda6584)/I(\mathrm{H}\alpha) \approx 0.4$ (Figure 9, right) that is a net evidence for the current star formation at this radius (Kewley et al. 2006). Interestingly, the color of *this* ring is not blue; it is even red to the west from the nucleus (Figure 9, left). Evidently, the star-forming ring at the outer edge of the bulge of NGC 3626 is buried by a large amount of dust. It is a little surprising that the blue knot is still seen quite clearly in $3''$ to the east of the nucleus, and the more distant H II region (a part of the star-forming ring) is hidden by the bulge and is not seen. Perhaps the warping of the gaseous disk plane in the center of the galaxy that has been revealed by the kinematical data (Figure 6) is a real geometrical distortion.

To see the history of star formation in the center of NGC 3626 in more detail, we present the Lick index maps derived from the SAURON data in Figure 10 and from the MPFS data in Figure 11. One can see immediately that the maps contain a lot of compact features which have been eliminated by azimuthal averaging in Figure 7. At the Hβ map *not* corrected for the emission, a ring of intense current star formation is outstanding by the negative values of the measured index. However, besides this outstanding feature, we note a prominent peak of the Hβ absorption-line index in $4''$–$5''$ to the northwest of the nucleus, close to one of the bluest spots in the $(B-V)$ color map of Figure 9 (left). We have found a counterpart to this feature at the

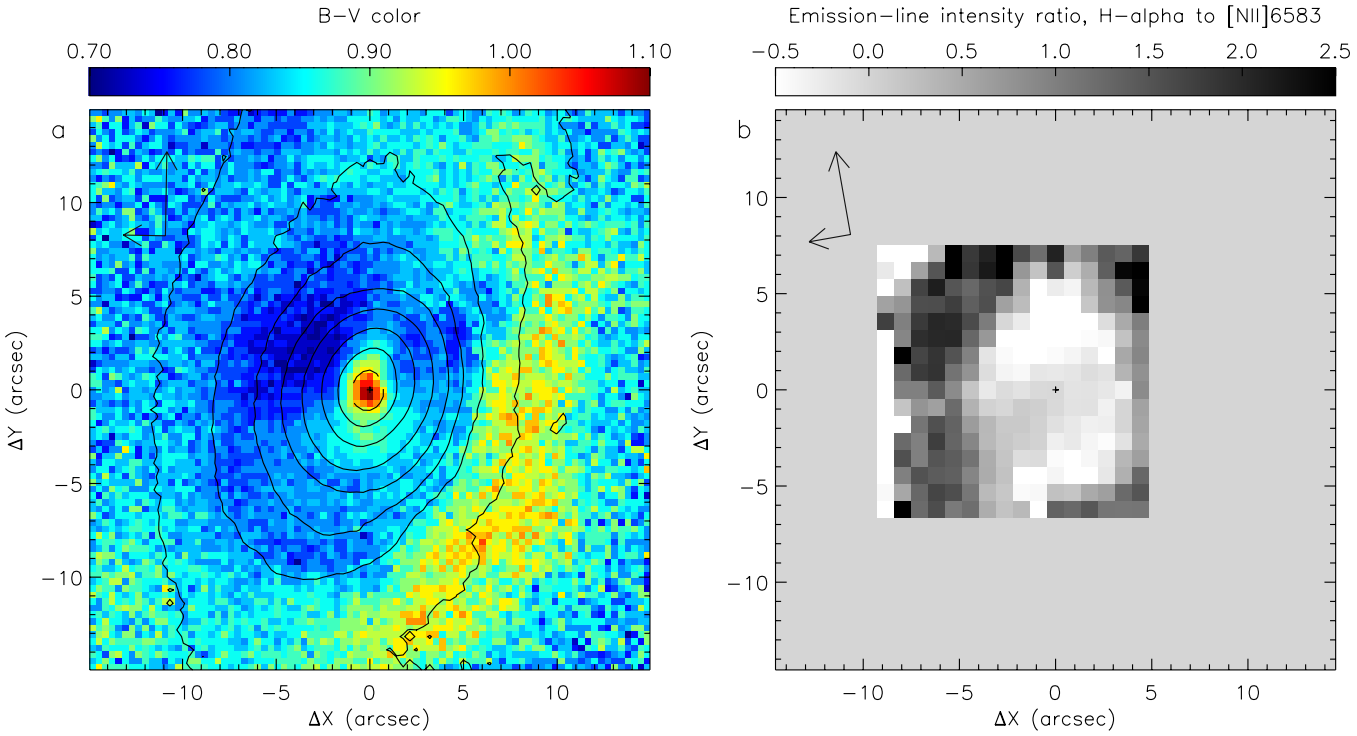

Figure 9. The *B*–*V* color map (left) and the map of the Hα to [N II] λ6584 emission-line ratio (right) for the central part of NGC 3626. The negative ratios mean that Hα here is an absorption line. The long arrow is directed toward the north, and the short one is directed toward the east.

(A color version of this figure is available in the online journal.)

Mgb map—it is a local minimum of the magnesium index. The analysis of the stellar population properties of this local "spot" with the MPFS data at the index–index diagrams reveals that it does not differ by an age but is somewhat less metal rich than its surroundings. Keeping in mind the considerable counterrotating gas content of NGC 3626, we can speculate that near the nucleus we may see a remnant of the merged dwarf galaxy, more specifically, the densest part of it which has spiraled through the whole disk of NGC 3626 during a few Gyrs after merging. The spot of the high stellar velocity dispersion somewhat farther from the center may be the precessing, less dense stellar "tail" of the merged satellite. The concentric elliptical rings of the young blue stars and of the Hα emission tracing the current star formation may be consequences of the interaction between accreted counterrotating gas and the prograde pre-existing gas of NGC 3626, as in NGC 3593 (Corsini et al. 1998). An alternative explanation of the ring structure similar to that observed in NGC 3626 is proposed by numerical simulations of close passages of galaxies by Tutukov & Fedorova (2006). The concentric stellar rings are formed when a companion moves in the equatorial plane in the direction opposite to the rotation of the studied galaxy (see their Figure 3). The large-scale gas counterrotation observed in NGC 3626 suggests just such a geometry of the galactic interaction. Interestingly, the radial concentration of star formation in NGC 3626 shifts with time: the star-forming ring expands slowly outward.

6. CONCLUSIONS AND BRIEF DISCUSSION

Both NGC 3599 and NGC 3626 are lenticular galaxies at the outskirts of the X-ray bright group. They are located beyond the dense intragroup medium area. In contrast to the "old" lenticular galaxy NGC 3607—the central galaxy of the group—they are "young" lenticular galaxies: the mean ages of the central stellar populations are less than 2 Gyr in both galaxies. If we relate the age of the last star formation in the nuclei to the galaxy transformation from spirals, these events occurred rather recently compared to the dynamical timescale, and some other signs still might be present and may help to identify these events. Indeed, both galaxies demonstrate complex features that are evidence of recent minor merging. First of all, the gas kinematics is quite decoupled from the stellar kinematics, and we may suggest that most of the gas that is observed in the central parts of the galaxies has been acquired recently. Both galaxies look isolated inside the group, so this is not mere accretion, but minor merging. The gas rotation planes are strongly warped, and at some distances from the center become almost polar with respect to the galactic large-scale disks; namely, NGC 3626 hosts the inner polar disk at the radii of $R < 500$ pc, whereas in NGC 3599 the ionized gas comes to significantly titled orbits out of $R \sim 200$ pc.

Near the very center in NGC 3599 and beyond some radii in NGC 3626, the gas rotation planes come closer to the main galactic planes, and the presence of star-forming nuclear rings in both galaxies can perhaps be explained by the accreted gas interaction with the primordial gas of the galaxies, as is the case in NGC 3593 (Corsini et al. 1998) or Arp 212 (Moiseev 2008). Moreover, the geometry of the gaseous disk in NGC 3599 looks just like a picture observed in Arp 212: the orbits of gas clouds are coplanar with a stellar disk in the circumnuclear regions and become warped (may be polar) at larger distances from the center. First of all, the compressed primordial gas has to be exhausted by the recent star formation, and the accreted counterrotating gas is left to be observed. Later, the counterrotating gas would also be reprocessed into stars, and we will see a counterrotating stellar component as is now seen in NGC 3593 (Bertola et al. 1996).

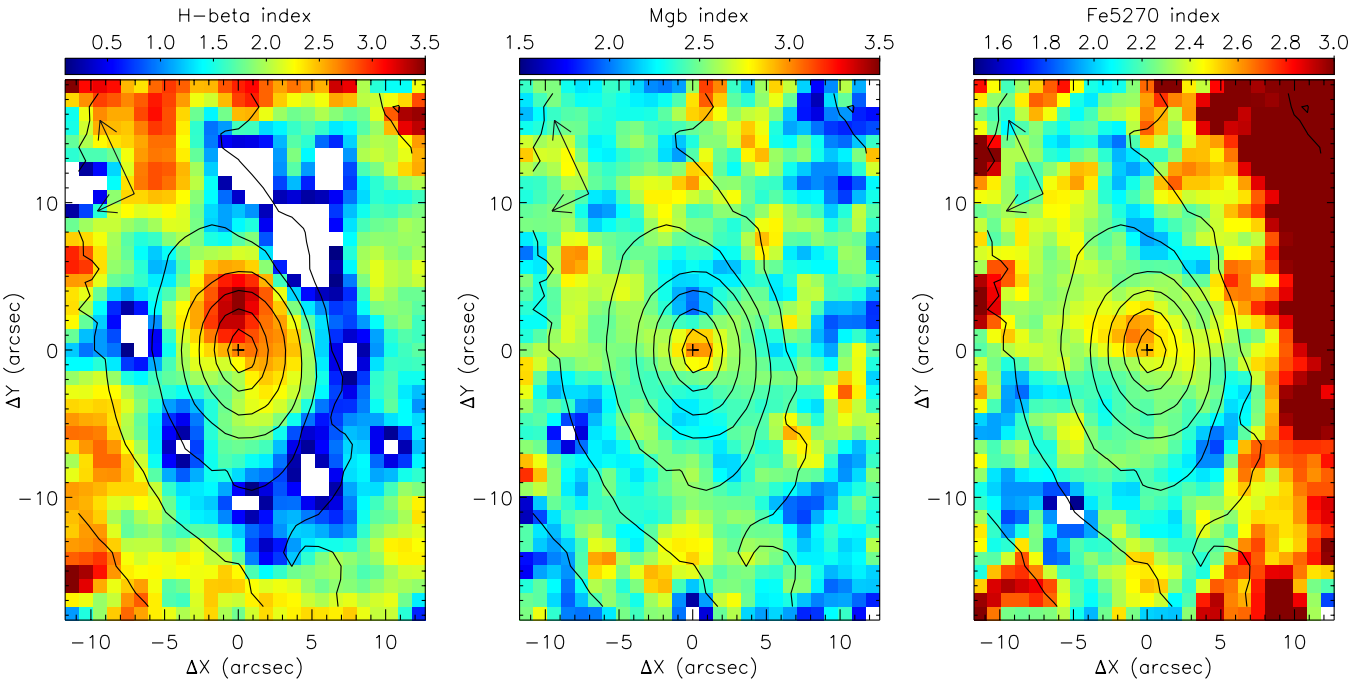

Figure 10. Lick index maps for the central part of NGC 3626 derived from the SAURON data: Hβ (left), Mgb (middle), Fe5270 (right). The long arrow is directed toward the north, and the short one is directed toward the east.

(A color version of this figure is available in the online journal.)

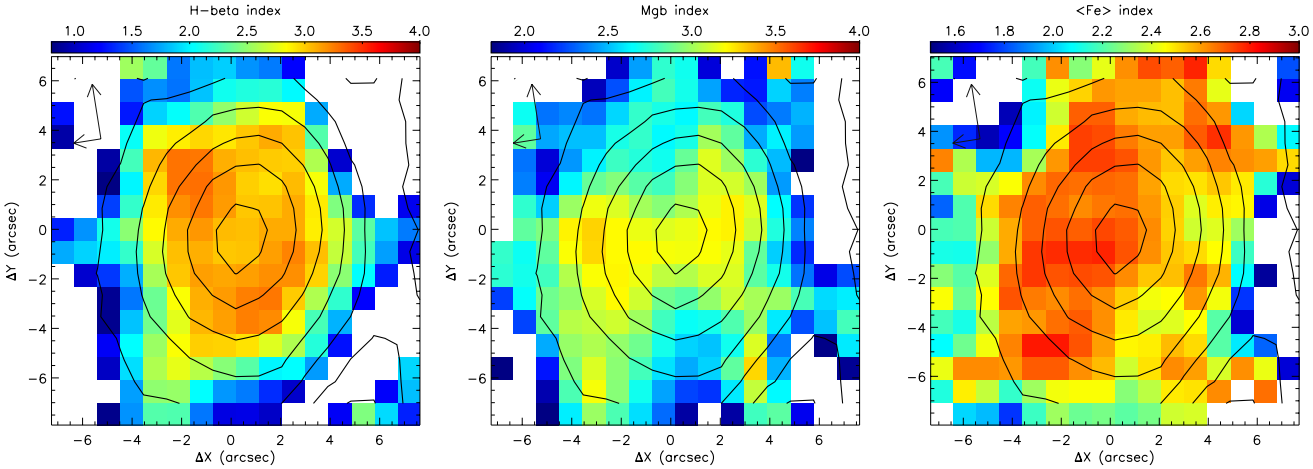

Figure 11. Lick index maps for the central part of NGC 3626 derived from the MPFS data: Hβ (left), Mgb (middle), ⟨Fe⟩ (right). The long arrow is directed toward the north, and the short one is directed toward the east.

(A color version of this figure is available in the online journal.)

NGC 3626, a large galaxy, has a huge amount of extended H I gas, while NGC 3599, a dwarf, has not. The extended gaseous disk of NGC 3626 counterrotates the stars, and if their rotation planes are coplanar, we can recall the simulations of an isolated stellar-gaseous disk by Friedli & Benz (1993) where initially counterrotating gas begins to inflow because of the bar and forms a stable highly inclined ring near the center due to vertical resonance effects. Though both galaxies are classified as SA (non-barred), their large-scale structures reveal multi-tiered stellar disks, and the inner disks in both galaxies are evidently oval. Therefore, we may suggest that the bars were present some time ago, but have now dissolved, or almost dissolved; dynamical simulations demonstrate that dissolving bars leave weakly oval stellar disks after their dissolution (Berentzen et al. 2006). The current star-forming ring in NGC 3626 may then be related to the inner Lindblad resonance of this dissolving bar.

The whole scenario of the galaxy transformations from spirals into lenticulars may include the following sequence of related events: first, a minor merger occurs, then the acquired gas and stars inflow to the center, the large-scale stellar disks develop bars and are heated, and the gas is compressed near the center and exhausted by the intense induced star formation. After a few Gyrs, we have typical lenticular galaxies, except for their unrelaxed gas behavior. Within such a scenario, the main mechanism of the lenticular galaxy formation is gravitational and not at all related to the intragroup hot medium impact.

We thank Prof. V. L. Afanasiev for supporting the Multi-Pupil Fiber Spectrograph of the 6 m telescope and for taking part in some of the observations from which data are used in this work. The 6 m telescope is operated under the financial

support of the Science Ministry of Russia (registration number 01-43). During our data analysis we used the Lyon-Meudon Extragalactic Database (LEDA) supplied by the LEDA team at the CRAL-Observatoire de Lyon (France) and the NASA/IPAC Extragalactic Database (NED) operated by the Jet Propulsion Laboratory, California Institute of Technology under contract with the National Aeronautics and Space Administration. This research is partly based on data obtained from the Isaak Newton Group Archive which is maintained as part of the CASU Astronomical Data Centre at the Institute of Astronomy, Cambridge, on observations made with the NASA/ESA *Hubble Space Telescope*, obtained from the data archive at the Space Telescope Science Institute, which is operated by the Association of Universities for Research in Astronomy, Inc., under NASA contract NAS 5-26555, and on SDSS data. Funding for the Sloan Digital Sky Survey (SDSS) and SDSS-II has been provided by the Alfred P. Sloan Foundation, the Participating Institutions, the National Science Foundation, the U.S. Department of Energy, the National Aeronautics and Space Administration, the Japanese Monbukagakusho, and the Max Planck Society, and the Higher Education Funding Council for England. The SDSS Web site is http://www.sdss.org/. The work on the study of multi-tiered disk galaxies is supported by the grants of the Russian Foundation for Basic Researches number 07-02-00229a and number 09-02-00870a.

REFERENCES

Adelman-McCarthy, J., et al. 2008, ApJS, 175, 297
Afanasiev, V. L., Dodonov, S. N., & Moiseev, A. V. 2001, in Stellar Dynamics: From Classic to Modern, ed. L. P. Osipkov & I. I. Nikiforov (Saint Petersburg: Saint Petersburg Univ. Press), 103
Afanasiev, V. L., & Moiseev, A. V. 2005, Astron. Lett., 31, 193
Afanasiev, V. L., & Sil'chenko, O. K. 2007, Astron. Astrophys. Trans., 26, 311
Bacon, R., et al. 1995, A&AS, 113, 347
Bacon, R., et al. 2001, MNRAS, 326, 23
Balinskaya, I. S., & Sil'chenko, O. K. 1993, Bull. SAO, 35, 43
Berentzen, I., Shlosman, I., & Jogee, S. 2006, ApJ, 637, 582
Bertola, F., Cinzano, P., Corsini, E. M., Pizzella, A., Persic, M., & Salucci, P. 1996, ApJ, 458, L67
Burgess, A. 1958, MNRAS, 118, 477
Ciri, R., Bettoni, D., & Galletta, G. 1995, Nature, 375, 661
Corsini, E. M., Pizzella, A., Funes, J. G., Vega Beltran, J. C., & Bertola, F. 1998, A&A, 337, 80
de Souza, R. E., Gadotti, D. A., & dos Anjos, S. 2004, ApJS, 153, 411
Dressler, A., et al. 1997, ApJ, 490, 577
Elmegreen, B. G., & Elmegreen, D. M. 1985, ApJ, 288, 438
Elmegreen, B. G., Elmegreen, D. M., Chromey, F. R., Hasselbacher, D. A., & Bissell, B. A. 1996, AJ, 111, 2233
Erwin, P., Pohlen, M., & Beckman, J. E. 2008, AJ, 135, 20
Esquej, P., et al. 2008, A&A, 489, 543
Fasano, G., Poggianti, B. M., Couch, W. J., Bettoni, D., Kjaergaard, P., & Moles, M. 2000, ApJ, 542, 673
Friedli, D., & Benz, W. 1993, A&A, 268, 65
Garcia-Burillo, S., Sempere, M. J., & Bettoni, D. 1998, ApJ, 502, 235
Haynes, M. P., Jore, K. P., Barrett, E. A., Broeils, A. H., & Murray, B. M. 2000, AJ, 120, 703
Just, D. W., Zaritsky, D., Sand, D. J., Desai, V., & Rudnick, G. 2010, ApJ, 711, 192
Kewley, L. J., Groves, B., Kauffmann, G., & Heckman, T. 2006, MNRAS, 372, 961
Kuntschner, H., et al. 2006, MNRAS, 369, 497
Laurikainen, E., Salo, H., & Buta, R. 2005, MNRAS, 362, 1319
Magrelli, G., Bettoni, D., & Galletta, G. 1992, MNRAS, 256, 500
Mahdavi, A., Bohringer, H., Geller, M., & Ramella, M. 2000, ApJ, 534, 114
Moiseev, A. V. 2008, Astrophys. Bull., 63, 201
Moiseev, A. V., Valdes, J.-R., & Chavushyan, V. H. 2004, A&A, 421, 433
Mulchaey, J. S., Davis, D. S., Mushotzky, R. F., & Burstein, D. 2002, ApJS, 145, 39
Pohlen, M., & Trujillo, I. 2006, A&A, 454, 759
Ramella, A., Pisani, A., & Geller, M. J. 1997, AJ, 113, 483
Sil'chenko, O. K. 1997, Astron. Rep., 41, 567
Sil'chenko, O. K. 2006, ApJ, 641, 229
Sil'chenko, O. K., & Afanasiev, V. L. 2008, Astron. Rep., 52, 875
Sil'chenko, O. K., Afanasiev, V. L., Chavushyan, V. H., & Valdes, J.-R. 2002, ApJ, 577, 668
Sil'chenko, O. K., Moiseev, A. V., Afanasiev, V. L., Chavushyan, V. H., & Valdes, J.-R. 2003, ApJ, 591, 185
Startseva, M. A., Sil'chenko, O. K., & Moiseev, A. V. 2009, Astron. Rep., 53, 1101
Stasinska, G., & Sodré, I., Jr. 2001, A&A, 374, 919
Thomas, D., Maraston, C., & Bender, R. 2003, MNRAS, 339, 897
Tonry, J. L., Dressler, A., Blakeslee, J. P., Ajhar, E. A., Fletcher, A. B., Luppino, G. A., Metzger, M. R., & Moore, Ch. B. 2001, ApJ, 546, 681
Tutukov, A. V., & Fedorova, A. V. 2006, Astron. Rep., 50, 785
Veilleux, S., & Osterbrock, D. E. 1987, ApJS, 63, 295
Wilman, D. J., Oemler, A., Mulchaey, J. S., McGee, S. L., Balogh, M. L., & Bower, R. G. 2009, ApJ, 692, 298
Worthey, G., Faber, S. M., Gonzàlez, J. J., & Burstein, D. 1994, ApJS, 94, 687
Wozniak, H., Friedli, D., Martinet, L., Martin, P., & Bratschi, P. 1995, A&AS, 111, 115